Efficient imaging of single-hole electromagnetic data

Ki Ha Lee[1], Hee Joon Kim[2], and Mike Wilt[3]

Abstract

The extended Born, or localized nonlinear (LN) approximation, of integral equation (IE) solution has been applied to inverting single-hole electromagnetic (EM) data using a cylindrically symmetric model. The extended Born approximation is less accurate than a full solution but much superior to the simple Born approximation. When applied to the cylindrically symmetric model with a vertical magnetic dipole source, however, the accuracy of the extended Born approximation is shown to be greatly improved because the electric field is scalar and continuous everywhere. One of the most important steps in the inversion is the selection of a proper regularization parameter for stability. The extended Born solution provides an efficient means for selecting an optimum regularization parameter, because the Green's functions, the most time consuming part in IE methods, are repeatedly re-usable at each iteration. In addition, the IE formulation readily contains a sensitivity matrix, which can be revised at each iteration at little expense. In this paper we show inversion results using synthetic and field data. The result from

[1] Ernest O. Lawrence Berkeley National Laboratory, Berkeley CA 94720, U.S.A., KHLee@lbl.gov

[2] Pukyong National University, Pusan 608-737, Korea, hejkim@pknu.ac.kr

[3] ElectroMagnetic Instruments, Inc., Richmond CA 94805, U.S.A., mwilt@slb.com

field data is compared with that of a 3-D inversion scheme.

Key words: single-hole, extended Born approximation, cylindrical symmetry, inversion

Introduction

High-resolution imaging of electrical conductivity has been the subject of many studies in cross-hole tomography using electromagnetic (EM) fields (Zhou, 1989; Zhou et al., 1993; Wilt et al., 1995; Alumbaugh and Morrison, 1995; Newman, 1995; Alumbaugh and Newman, 1997). Although the theoretical understanding and associated field practices for cross-hole EM methods are relatively mature, these techniques are costly and sometimes it is difficult to find two adjacent boreholes for cross-hole surveys. The cost can be greatly reduced if a single-hole survey method could be developed.

The main advantage of integral equation (IE) method in comparison with the finite difference (FD) and/or the finite element (FE) methods, is the fast and accurate simulation of compact 3-D bodies in a layered background (Hohmann, 1975). The FD and FE methods are

suitable for modeling EM fields in complex structures with large-scale conductivity variations. In principle, the IE method can handle these models too, but the huge demand on computer resources places a practical limit on its use. This is because of the full matrix arising from IE formulation. Another advantage of the IE method over the FD or FE method is its greater suitability for inversion. IE formulation readily contains a sensitivity matrix, which can be revised at each inversion iteration at little expense. With FD or FE, in contrast, the sensitivity matrix has to be recomputed at each iteration at a cost nearly equal to that of full forward modeling. The IE method, however, has to overcome severe practical limitations imposed on the numerical size of the anomalous domain for inversion purposes. In this direction, several approximate methods, such as the localized nonlinear (LN) approximation (Habashy et al., 1993) and quasi-linear approximation (Zhdanov and Fang, 1996), have been developed recently. In this paper we exploit the advantage of the LN approximation with applications to single-hole inversion of EM data.

Approach

Maxwell's equations with an e^{+iwt} time dependence, neglecting displacement currents,

are written as

$$\tilde{\nabla} \times \mathbf{E}(\mathbf{r}) = -i\omega\mu\mathbf{H}(\mathbf{r}), \tag{1}$$

$$\tilde{\nabla} \times \mathbf{H}(\mathbf{r}) = \sigma(\mathbf{r})\mathbf{E}(\mathbf{r}) + \mathbf{J}_s(\mathbf{r} - \mathbf{r}_s), \tag{2}$$

where $\mathbf{J}_s$ is the impressed current source at $\mathbf{r}_s$. We assume the magnetic permeability μ is constant and is equal to that of free space. The electrical conductivity σ is heterogeneous and it may be divided into

$$\sigma(\mathbf{r}) = \sigma_b + \Delta\sigma(\mathbf{r}), \tag{3}$$

where the subscript 'b' indicates the background. The conductivity of the background medium is assumed uniform throughout this paper. The differential equation for the secondary electric field is derived from equations (1) and (2) as

$$\tilde{\nabla} \times \tilde{\nabla} \times \mathbf{E}(\mathbf{r}) + i\omega\mu\sigma(\mathbf{r})\mathbf{E}(\mathbf{r}) = -i\omega\mu\mathbf{J}_s(\mathbf{r}), \tag{4}$$

and the numerical solution for the electric field may be obtained using either the finite-element or

the finite-difference method. Alternatively, numerical solution may be obtained using the integral equation method involving the Green's function that satisfies

$$\tilde{\nabla} \times \tilde{\nabla} \times \mathbf{G}^{\mathrm{EJ}}\left(\mathbf{r}\text{-}\mathbf{r}'\right) + iwms_b \mathbf{G}^{\mathrm{EJ}}\left(\mathbf{r}\text{-}\mathbf{r}'\right) = \mathbf{I}d\left(\mathbf{r}'\text{-}\mathbf{r}_s\right). \tag{5}$$

The symbol **I** is the identify tensor. The superscript 'EJ' signifies that the Green's function translates current source, **J**, to electric field **E**. Each vector component of the Green's tensor $\mathbf{G}^{\mathrm{EJ}}\left(\mathbf{r}\text{-}\mathbf{r}'\right)$ is the vector electric field at **r** due to a point source at **r′** with its current density of $-\left(i\omega\mu\right)^{-1}$ Amp/m^2, polarized in *x*, *y*, and *z*, respectively. Using equations (4) and (5), one can derive an integral equation for the electric field

$$\mathbf{E}(\mathbf{r}) = \mathbf{E}_{\mathrm{b}}(\mathbf{r}) - i\omega\mu \int_{\mathrm{V}} \mathbf{G}^{\mathrm{EJ}}(\mathbf{r}\text{-}\mathbf{r}') \cdot \Delta\sigma\left(\mathbf{r}'\right)\mathbf{E}\left(\mathbf{r}'\right) dv'. \tag{6}$$

The first term on the right is the background electric field that would exist in the presence of background medium only, and the term $\Delta\sigma\,\mathbf{E}$ inside the integral is called the scattering current (Hohmann, 1975).

The integral equation is nonlinear because the electric field inside the integral is function of the

conductivity. To obtain a numerical solution, the anomalous body is divided into a number of elements, and constant electric field is assigned to each element. Since Raiche (1974) first formulated the volume 3-D integral equation methods, many numerical solutions have been presented on this subject (Hohmann, 1988). The process involved in the volume integral equation methods requires computing time proportional to the cube of the number of cells used, and it quickly becomes impractical as the size of the inhomogeneity is increased to handle realistic problems.

For some important class of problems the complexity associated with the full 3-D problem can be reduced to something much simpler. A model whose electrical conductivity is cylindrically symmetric in the vicinity of a borehole is such an example. In order to preserve the cylindrical symmetry in the resulting EM field a horizontal loop current source, or a vertical magnetic dipole, may be considered in the borehole. In this case the problem is scalar when formulated using the azimuthal electric field E_φ, and the analogous integral equation is,

$$E_\varphi(\mathbf{r}) = E_{\varphi b}(\mathbf{r}) - 2\pi i\omega\mu \iint_{\rho' z'} G^{EJ}(\mathbf{r}\text{-}\mathbf{r}')\Delta\sigma(\mathbf{r}')E_\varphi(\mathbf{r}')\rho' d\rho' dz', \qquad (7)$$

where the position vector $\mathbf{r} = \vec{\rho} + \vec{z}$, and $\mathbf{r'} = \vec{\rho}' + \vec{z}'$. The electric field and Green's function are

both scalar, and the Green's function is given in the form of a Hankel transform (p219, Ward and Hohmann, 1988)

$$G^{\mathrm{EJ}}\left(\mathbf{r},\mathbf{r}'\right) = -\frac{1}{4\pi}\int_0^{\infty}\frac{e^{-u_b|z-z'|}}{u_b}\lambda J_1\left(\lambda\rho\right)J_1\left(\lambda\rho'\right)d\lambda\,, \tag{8}$$

where $u_b = \left(\lambda^2 + i\omega\mu\sigma_b\right)^{1/2}$. Since measurements are usually made for the magnetic field, equations (7) is reformulated to

$$H_z\left(\mathbf{r}\right) = H_{zb}\left(\mathbf{r}\right) - 2\pi i\omega\mu\iint_{\rho'z'} G^{\mathrm{HJ}}(\mathbf{r}-\mathbf{r}')\Delta\sigma\left(\mathbf{r}'\right)E_{\varphi}\left(\mathbf{r}'\right)\rho'\,d\rho'\,dz'\,, \tag{9}$$

where $G^{\mathrm{HJ}}(\mathbf{r},\mathbf{r}')$ translates scattering currents $\Delta\sigma\left(\mathbf{r}'\right)E_{\varphi}\left(\mathbf{r}'\right)$ at $\mathbf{r}'$ to magnetic field at $\mathbf{r}$. Using equations (7) through (9), one can obtain the integral equation solution by first dividing the (ρ,z) cross section into a number of elements, and formulate a system of equations for the electric field using pulse base function. Sena and Toksoz (1990) presented a cross-hole inversion study for permittivity and conductivity in cylindrically symmetric medium using high-frequency EM, and Alumbaugh and Morrison (1995) investigated cross-hole EM tomography using Born approximation and localized nonlinear (LN) approximation of Habashy et al. (1993).

Borehole access for geophysical survey in producing fields is very limited. For this reason, we consider an efficient single-hole EM imaging using the LN approximation. The LN approximation offers an efficient and reasonably accurate electric field solution without solving the full integral equation solution from equation (7). To do this the integral equation is first reformulated (Habashy et al., 1993) to

$$E_{\varphi}(\mathbf{r}) = E_{\varphi b}(\mathbf{r}) - 2\pi i\omega\mu E_{\varphi}(\mathbf{r}) \iint_{\rho' z'} G^{\mathrm{EJ}}(\mathbf{r}\text{-}\mathbf{r}')\Delta\sigma(\mathbf{r}')\,\rho'\,d\rho'\,dz' - 2\pi i\omega\mu \iint_{\rho' z'} G^{\mathrm{EJ}}(\mathbf{r}\text{-}\mathbf{r}')\Delta\sigma(\mathbf{r}')\left[E_{\varphi}(\mathbf{r}') - E_{\varphi}(\mathbf{r})\right]\rho'\,d\rho'\,dz',$$

or

$$E_{\varphi}(\mathbf{r}) + 2\pi i\omega\mu E_{\varphi}(\mathbf{r}) \iint_{\rho' z'} G^{\mathrm{EJ}}(\mathbf{r}\text{-}\mathbf{r}')\Delta\sigma(\mathbf{r}')\,\rho'\,d\rho'\,dz' = E_{\varphi b}(\mathbf{r}) - 2\pi i\omega\mu \iint_{\rho' z'} G^{\mathrm{EJ}}(\mathbf{r}\text{-}\mathbf{r}')\Delta\sigma(\mathbf{r}')\left[E_{\varphi}(\mathbf{r}') - E_{\varphi}(\mathbf{r})\right]\rho'\,d\rho'\,dz'.$$

If the electric field is continuous in the vicinity **r**, the contribution from the second integral may be small compared with the background electric field. This is because when **r′** approaches **r**, the difference in $\left[E_{\varphi}(\mathbf{r}') - E_{\varphi}(\mathbf{r})\right]$ is getting smaller, so the scattering current is effectively zero at the singular point. When **r′** moves away from **r** the contribution is also small because the Green's

function falls off rapidly. So for the type of problem where there is only the azimuthal electric field, we can get a good approximation even if we neglect the second integral entirely. As a result we get

$$E_{\varphi}(\mathbf{r})\left[1+2\pi i\omega\mu\iint_{\rho' z'} G^{\mathrm{EJ}}(\mathbf{r}\text{-}\mathbf{r}')\Delta\sigma(\mathbf{r}')\rho' d\rho' dz'\right]\approx E_{\varphi b}(\mathbf{r}),$$

from which, using

$$E_{\varphi}(\mathbf{r})\approx\gamma(\mathbf{r})E_{\varphi b}(\mathbf{r}), \tag{10}$$

where

$$\gamma(\mathbf{r})=\left[1+2\pi i\omega\mu\iint_{\rho' z'} G^{\mathrm{EJ}}(\mathbf{r}\text{-}\mathbf{r}')\Delta\sigma(\mathbf{r}')\rho' d\rho' dz'\right]^{-1}.$$

Substituting the approximate electric field solution into equation (9), we get the approximate magnetic field solution

$$H_z(\mathbf{r})\approx H_{zb}(\mathbf{r})-2\pi i\omega\mu\iint_{\rho' z'} G^{\mathrm{HJ}}(\mathbf{r}-\mathbf{r}')\Delta\sigma(\mathbf{r}')\left[\gamma(\mathbf{r}')E_{\varphi b}(\mathbf{r}')\right]\rho' d\rho' dz'. \tag{11}$$

To illustrate the efficiency and usefulness of the LN numerical solution, especially in single-hole application, let us consider a simple model consisting of a conductive ring about a borehole axis in a uniform whole space of 100 ohm-m resistivity. The cross section of the ring is a 3 m by 4 m rectangle as shown in Figure 1. We will let the transmitter-receiver offset (*a* in Figure 1), borehole-to-conductor distance (*b* in Figure 1), vertical distance between the transmitter and the top of the conductor (*c* in Figure 1), and the conductivity contrast (σ_2/σ_1) vary and find out how the LN approximated vertical magnetic field compares with the result obtained from the full finite-element method (FEM). Unless otherwise indicated the frequency used is 100 kHz throughout. Figure 2 shows the comparison in the secondary vertical magnetic field between the FEM (solid and broken lines) and the LN solutions for three different transmitter-receiver separations. We chose center of the body as z=0, and plots have been made at the transmitter-receiver midpoint. Conductivity contrast used is 10, and the borehole-to-conductor distance is 3 m. For all three separations; 4 m, 6 m, and 8 m, two solutions agree very well. More anomalies can be observed in the imaginary part. The anomaly also gets stronger for shorter source-receiver separations. At the separation of 4 m the imaginary part of the anomaly is 2.0×10^{-4} Amp/m, and it is about an 8% of primary field is 2.48×10^{-3} Amp/m (not shown here). Next, we consider responses by varying the borehole-to-conductor separation,

while the conductivity contrast and transmitter-receiver separation are fixed at 10 and 4 m, respectively. When the separation is small we anticipated that the LN approximation may not be as good, because the rapid changes in the electric field in the vicinity of the transmitter is not a favorable condition for LN approximation. Figure 3 confirms this is indeed the case. For the separation of 1 m, we see significant difference in the peak values of the real part between the FEM and LN solutions. The difference is less in the imaginary part. We are also interested in the quality of the LN solution when the conductivity of the body is increased. With the transmitter-receiver separation, borehole-to-conductor distance, and the transmitter to the top of the conductor distance fixed to 6 m, 3 m, and 4.5 m, respectively, the LN approximation is very good up to a conductivity contrast of 200 (Figure 4). The imaginary part of the LN solution starts deviating from the FEM solution beyond conductivity contrast of 200, while the real part still shows good agreement. Finally, the comparison is made for responses in frequency. Conductivity contrast, transmitter-receiver separation, and borehole-to-conductor distance are fixed at 10, 6 m, and 3 m, respectively, and the FEM and LN solutions are obtained for frequencies ranging from 200 Hz to 80 MHz. Two solutions show good agreement all the way up to 2 MHz (see details on the right of Figure 5).

Based on the encouraging results of the LN approximation, we decided to proceed to implement

the single-hole EM inversion. The measurement position is in the same borehole as the transmitter, so the radial distance ρ is zero. Upon dividing the inhomogeneity into *K* elements, the secondary magnetic field at the *i*-th receiver position in the borehole may be written as

$$H_{zi}^{s} \approx -2\pi i\omega\mu \sum_{k=1}^{K} \Delta\sigma_k \gamma_k E_{\varphi bk} \iint_{S_k} G^{\mathrm{HJ}}(\rho', z_i - z')\rho' d\rho' dz', \tag{12}$$

where the subscript *k* denotes the value at the *k*-th element. The corresponding Green's function for the magnetic field may be deduced from the electric field Green's function, equation (8), as

$$G^{\mathrm{HJ}}(\rho', z_i - z') = \frac{1}{4\pi i\omega\mu} \int_0^{\infty} \frac{e^{-u_b|z_i - z'|}}{u_b} \lambda^2 J_1(\lambda\rho') d\lambda . \tag{13}$$

For the inversion, the sensitivity of the magnetic field with respect to the change in conductivity can be easily obtained from equation (12). Taking derivative of the data with respect to the *j*-th conductivity parameter, and neglecting the dependence of the γ_j on $\Delta\sigma_j$, the sensitivity becomes

$$\frac{\partial}{\partial \sigma_j} H_{zi}^s \approx - 2\pi i \omega \mu \gamma_j E_{\varphi bj} \iint_{S_j} G^{\mathrm{HJ}}(\rho', z_i - z') \rho' d\rho' dz' , \tag{14}$$

which can be easily evaluated by integrating over the *j*-th element.

The inversion procedure starts with the data misfit $\left\| \mathbf{W}_d \left\{ \mathbf{H}(\sigma) - \mathbf{H}_d \right\} \right\|^2$, where all subscripts and superscripts have been dropped except for the subscript *d* denoting data. The data weighting matrix $\mathbf{W}_d$ is used to give relative weights to individual data. If we allow a perturbation $\delta\sigma$ to the conductivity the misfit will take a form $\left\| \mathbf{W}_d \left[\mathbf{H}(\sigma + \delta\sigma) - \mathbf{H}_d \right] \right\|^2$, and the total objective functional may be written as

$$\phi = \left\| \mathbf{W}_d \left[\mathbf{H}(\sigma + \delta\sigma) - \mathbf{H}_d \right] \right\|^2 + \lambda \left\| \mathbf{W}_\sigma \delta\sigma \right\|^2 \quad . \tag{15}$$

The second term is added to impose a smoothness constraint. $\mathbf{W}_\sigma$ is a weighting matrix and λ is the Lagrange multiplier that controls the trade-off between data misfit and the parameter smoothness. Expanding the misfit in $\delta\sigma$ using the Taylor series, discarding terms higher than the square term, and letting the variation of the functional with respect to $\delta\sigma$ equal to zero, we obtain a linear system of equations for the perturbation $\delta\sigma$

$$\left(\mathbf{J}^T\mathbf{W}_d^T\mathbf{W}_d\mathbf{J}+\lambda\mathbf{W}_\sigma^T\mathbf{W}_\sigma\right)\delta\sigma=-\mathbf{J}^T\mathbf{W}_d^T\mathbf{W}_d\left[\mathbf{H}(\sigma)-\mathbf{H}_d\right]. \quad (16)$$

Here, the entries of Jacobian matrix **J** are the sensitivity function given in equation (14). The stability of the inversion is largely controlled by requiring the conductivity to vary smoothly. Larger values of λ result in smooth and stable solutions at the expense of resolution. It even allows for the solution of grossly underdetermined problems (Tikhonov and Arsenin, 1977). In our single-hole inversion study, the Lagrange multiplier λ is progressively selected in the inversion process. The selection procedure starts with executing a given number, say *nl*, of inversions using *nl* different multipliers that are spaced appropriately. The same Jacobian is used at this step. As a result *nl* updated parameter sets are produced, followed by *nl* forward model calculations resulting in *nl* data misfits. Among these, we choose the model and parameter λ giving the lowest data misfit. In this selection scheme, integral equation (IE), or an approximate IE, modeling is quite attractive in speed because the Green's functions, the most time consuming part in IE methods, are repeatedly re-usable throughout the selection procedure.

To evaluate the performance of the extended Born inversion using LN approximation, we chose a conductivity model shown on the left of Figure 6. The model consists of two, one

conductive (1 S/m) and the other resistive (0.01 S/m), cylindrically symmetric bodies in a whole space of 0.1 S/m. A finite-element modeling (FEM) scheme is used to generate synthetic data. Using a vertical magnetic dipole as a source, vertical magnetic fields are computed at five source-receiver offsets of 4 m through 8 m at three frequencies of 12 kHz, 24 kHz and 42 kHz. Using 3-digit synthetic data generated by FEM, the inversion is started with an initial model of 0.25 S/m uniform whole space. In this test we used $nl = 3$ in each iteration to select parameter update and Lagrange multiplier. After 6 iterations, the two bodies are clearly reconstructed as shown on the right of Figure 6. The recovered conductivity is found to be nearly the same in the conductive body but is overestimated in the resistive body. The inversion process is quite stable as shown in Figure 7, where the misfit in rms misfit decreased from the initial guess of 0.478 (not shown) to under 0.01 after 8 iterations. The rms misfit of 0.01 is assumed to be a target misfit level because the error level in the synthetic responses is estimated to be about 1 %.

Electromagnetic Inctruments Inc. (EMI) conducted a field test of the newly built Geo-BILT tool at Lost Hills oil field in southern California operated by Chevron USA in May 2001. LBNL obtained the data to evaluate them for future development of the 3-D approximate inversion scheme. As part of the final evaluation of 2-D inversion code, we conducted inversion of the data using only the M_z-H_z data (Figure 8) and the result is shown in Figure 9. Initial model used is 0.25 S/m uniform whole space, and after 6 iterations the rms is reduced to less than 1%

(Figure 10). The conductive zone near the borehole in all depths appears to be an artifact. This is apparent if we compare the 2-D inversion result with that of a 3-D inversion (Wilt et al., 2002) of the same section shown on the right of Figure 9. The 3-D inversion used all three-component magnetic fields as data from vertical magnetic dipole sources along the borehole. The 3-D result shown here is only one cross section (easting direction) across the borehole, and it shows resistive zone around the borehole at the depth of 1680 ft. Similar resistive zone appeared at the same depth after 2nd iteration of the 2-D inversion. Further iterations reduce the rms but, because of the overfitting, artifacts started to appear as is apparent from the result of 6th iteration. Further indication of the overfitting can be seen in Figure 11 in which the magnetic fields generated from inverted model are shown to be perfectly fitting with the field data. Here, only the imaginary part is compared because the real part has very little anomaly. Computing time required for the 2-D approximate inversion is about 30 minutes compared to 3 to 5 days for the 3-D inversion on a PC computer (Wilt et al, 2002).

Conclusions

A computationally efficient inversion scheme has been developed using localized nonlinear (LN) approximation to analyze EM fields obtained in a single-hole environment. The

medium is assumed to be cylindrically symmetric about the borehole, and to maintain the symmetry vertical magnetic dipole source is used throughout. The efficiency and robustness of an inversion scheme is very much dependent on the proper use of Lagrange multiplier, which is often provided manually to achieve a desired convergence. We have developed an automatic Lagrange multiplier selection scheme, which will enhance the utility of the inversion scheme in handling field data. The 2-D inversion scheme was tested using field data and the result was compared with the conductivity image generated by a 3-D inversion with a reasonable agreement. For an approximate inversion scheme such as the one developed here, one needs to be careful not to overfit the data to avoid undesirable artifacts in the reconstructed image.

Acknowledgments

This work was supported by the Assistant Secretary for Energy Efficiency and Renewable Energy, Office of Wind and Geothermal Technologies of the U.S. Department of Energy under Contract No. DE-AC03-76SF00098. We would like to thank Michael Morea, Chevron USA Production Company, and the US Department of Energy, National Petroleum Technology Office, (Class III Field Demonstration Project DE-FC22-95BC14938) for allowing us to publish this

data. The research was partially supported by Korea Research Foundation (KRF-2000-015-DP0431).

References

Alumbaugh, D. L. and Morrison, H. F., Theoretical and practical considerations for crosswell electromagnetic tomography assuming a cylindrical geometry, *Geophysics*, *60*, 846-870, 1995.

Alumbaugh, D. L., and Newman, G. A., Three-dimensional massively parallel electromagnetic inversion –II. Analysis of crosswell electromagnetic experiment, *Geophys. J. Int*., *128*, 355-363, 1997.

Constable, S. C., Parker, R. L., and Constable, C. G., Occam's inversion: A practical algorithm for generating smooth model from EM sounding data, *Geophysics*, *52*, 289-300, 1987.

Habashy, T. M., Groom, R. M., and Spies, B. R., Beyond the Born and Rytov approximations: a nonlinear approach to electromagnetic scattering, *J. Geophys. Res., 98*, 1795-1775,1993.

Hohmann, G. W., Three-dimensional induced polarization and EM modeling, *Geophysics, 40*, 309-324, 1975.

Hohmann, G. W., Numerical modeling for electromagnetic methods of geophysics, in

Electromagnetic methods in applied geophysics, Investigations in Geophysics 3, Vol. 1: Soc. Expl. Geophys, edited by M. N. Nabighian, 1988.

Newman, G. A., Crosswell electromagnetic inversion using integral and differential equations, *Geophysics, 60*, 899-911, 1995.

Raiche, A. P., An integral equation approach to 3D modeling, *Geophys. J. Roy. Astr. Soc., 36,* 363-376, 1974.

Sena, A. G., and Toksoz, M. N., Simultaneous reconstruction of permittivity and conductivity for crosshole geometries, *Geophysics, 55*, 1302-1311, 1990.

Tikhonov, A. N., and Arsenin, V. Y., Solutions to Ill-Posed Problems, John Wiley and Sons, Inc., 1977.

Ward, S. H., and Hohmann, G.. W., Electromagnetic Theory for Geophysical Applications in Electromagnetic methods in applied geophysics, Investigations in Geophysics 3, Vol. 1: Soc. Expl. Geophys, edited by M. N. Nabighian, 1988.

Wilt, M. J., Alumbaugh, D. L., Morrison, H. F., Becker, A., Lee, K. H., and Deszcz-Pan, M., Crosshole electromagnetic tomography: System design considerations and field results: *Geophysics, 60*, 871-885, 1995.

Wilt, M. J., Mallan, R., Kasameyer, P., and Kirkendall, B., 3D extended logging for geothermal resources: Field trials with the Geo-BILT system, Proceedings, Twenty-seventh Workshop

on Geothermal Reservoir Engineering, Stanford University, Stanford, California, January 28-30, SGP-TR-171, 2002.

Zhdanov, M. S., and Fang, S., Quasi-linear approximation in 3-D EM modeling, *Geophysics, 61*, 646-665, 1996.

Zhou, Q., Becker, A., and Morrison, H. F., Audio-frequency electromagnetic tomography in 2-D, *Geophysics, 58*, 482-495, 1993.

Figure Captions

Figure 1. A cylindrically symmetric model. The inhomogeneous body with a cross-section of 3 by 4 m is cylindrically symmetric about the borehole in which source and receiver are inserted. The parameters *a*, *b*, and *c* represents the source-receiver, horizontal hole-body and vertical source-body separations, respectively.

Figure 2. The effect of source-receiver separation on the vertical component of secondary magnetic fields. Operating frequency is 10^5 Hz. The 0.1 S/m body is located in a whole space of 0.01 S/m at 3 m horizontally away from the borehole.

Figure 3. The effect of hole-body separation on the vertical component of secondary magnetic fields. The operating frequency is 10^5 Hz, the conductivity contrast between body and background is 10, and the source receiver separation is 4 m.

Figure 4. The effect of operation frequency on the secondary magnetic fields. The source-receiver separation is 6 m. The 0.1 S/m body is located in a whole space of 0.01 S/m at 3 m horizontally away from the borehole.

Figure 5. The effect of conductivity contrast between body and background on the secondary magnetic fields. The operating frequency is 10^5 Hz, the source-receiver separation is 6 m and the horizontal hole-body separation is 3 m.

Figure 6. Inversion of synthetic model. The model (left) used to calculate synthetic data for inversion test consists of two bodies, of 1 S/m and 0.01 S/m, located in a whole-space of 0.1 S/m. An image of two conductors reconstructed from the synthetic data after 8th iteration.

Figure 7. Convergence in rms for the synthetic model inversion.

Figure 8. Vertical magnetic field data obtained in the borehole OBC1 at two offsets, 2 m and 5 m, at the frequency of 6 kHz. Source used is vertical magnetic dipole. These data sets are used to image electrical resistivity as shown in Figure 9.

Figure 9. Resistivity imaging derived from the 2-D inversion of data obtained from Chevron USA. The model started with uniform conductivity of 0.25 S/m, and after eight iterations, the misfit in terms of rms (shown as fractional numbers after the number of iteration shown at the top of each image) converged to about 1%. The image shown on the right is from a 3-D inversion of three-component data with vertical magnetic dipole source (Wilt et al., 2002)

Figure 10. Convergence in rms misfit and associated Lagrange multiplier as a function of iteration during the inversion of field data.

Figure 11. Comparison of field data and inverted model responses in the imaginary component.

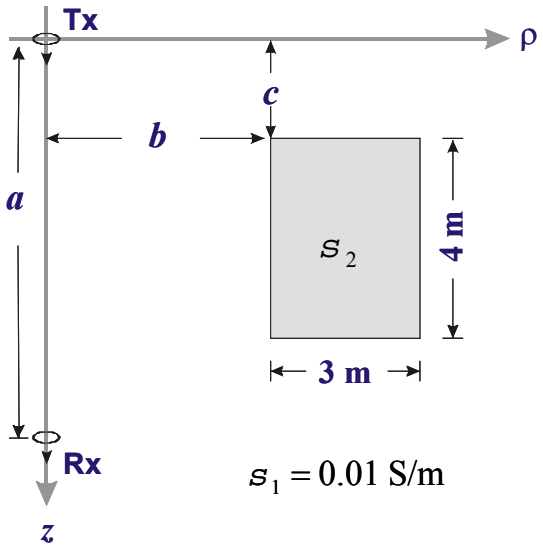

Figure 1. A cylindrically symmetric model. The inhomogeneous body with a cross-section of 3 by 4 m is cylindrically symmetric about the borehole in which source and receiver are inserted. The parameters *a*, *b*, and *c* represents the source-receiver, horizontal hole-body and vertical source-body separations, respectively.

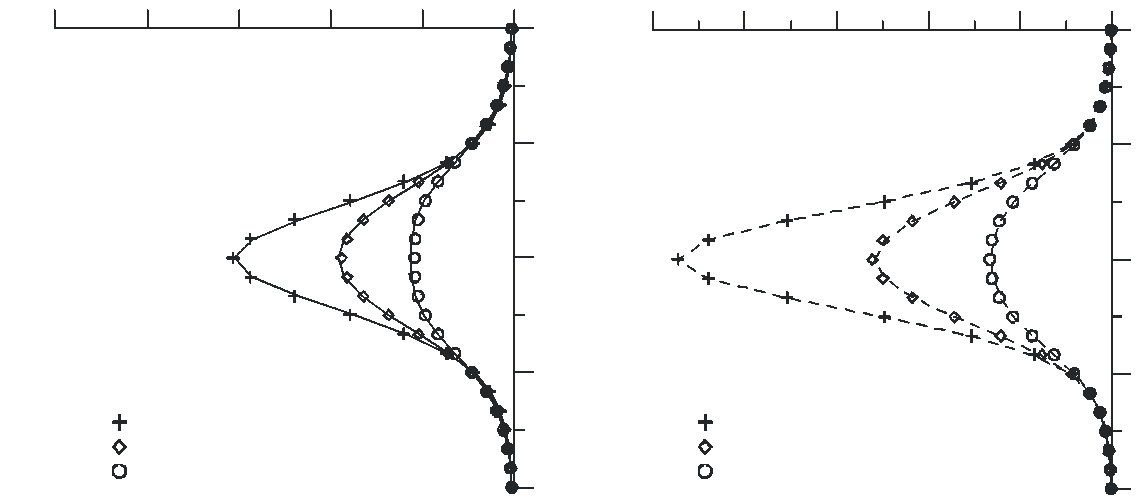

Figure 2. The effect of source-receiver separation on the vertical component of secondary magnetic fields. Operating frequency is 10^5 Hz. The 0.1 S/m body is located in a whole space of 0.01 S/m at 3 m horizontally away from the borehole.

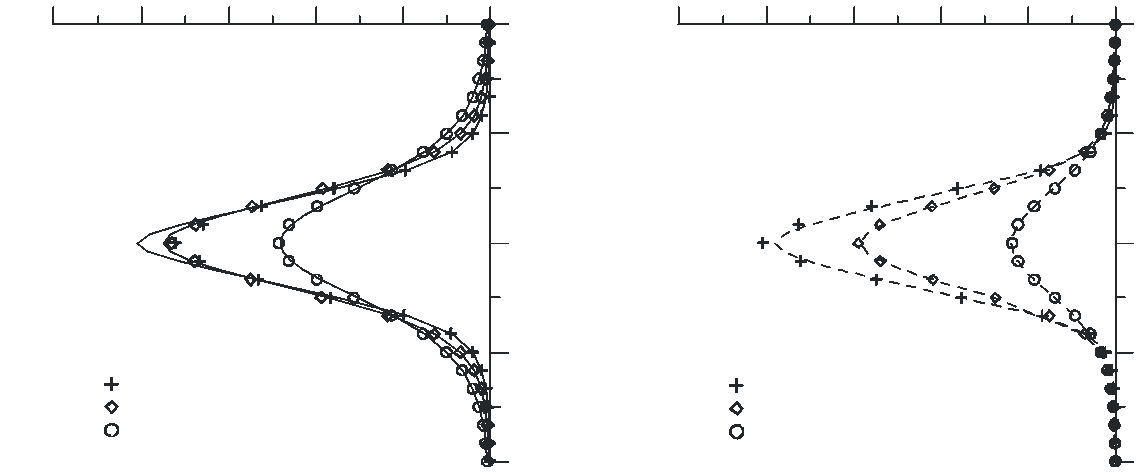

10^5 Hz, $\sigma_2/\sigma_1 = 10$, $a = 4$ m

Figure 3. The effect of hole-body separation on the vertical component of secondary magnetic fields. The operating frequency is 10^5 Hz, the conductivity contrast between body and background is 10, and the source receiver separation is 4 m.

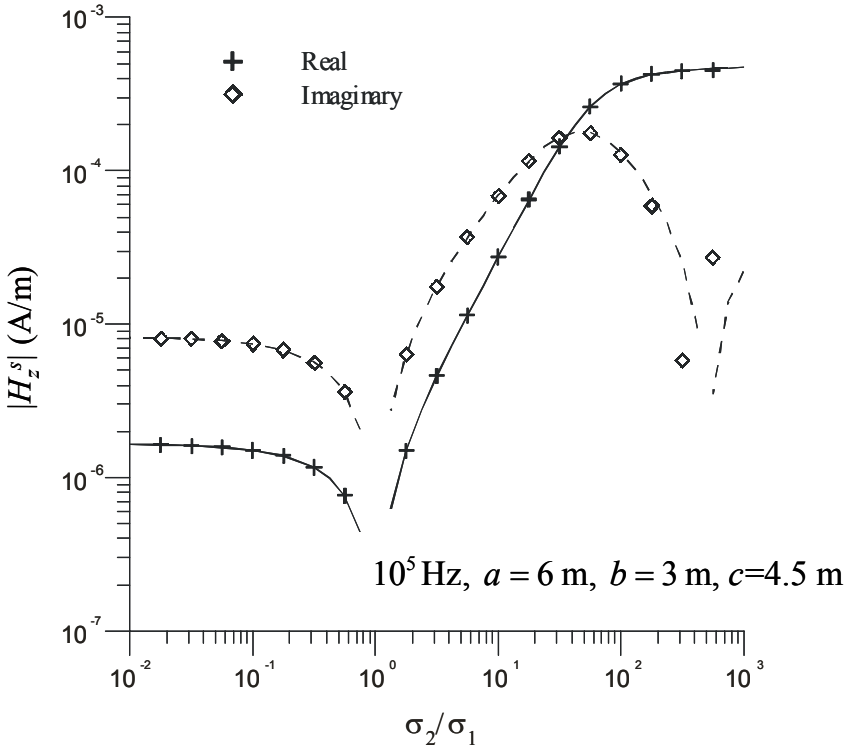

Figure 4. The effect of operation frequency on the secondary magnetic fields. The source-receiver separation is 6 m. The 0.1 S/m body is located in a whole space of 0.01 S/m at 3 m horizontally away from the borehole.

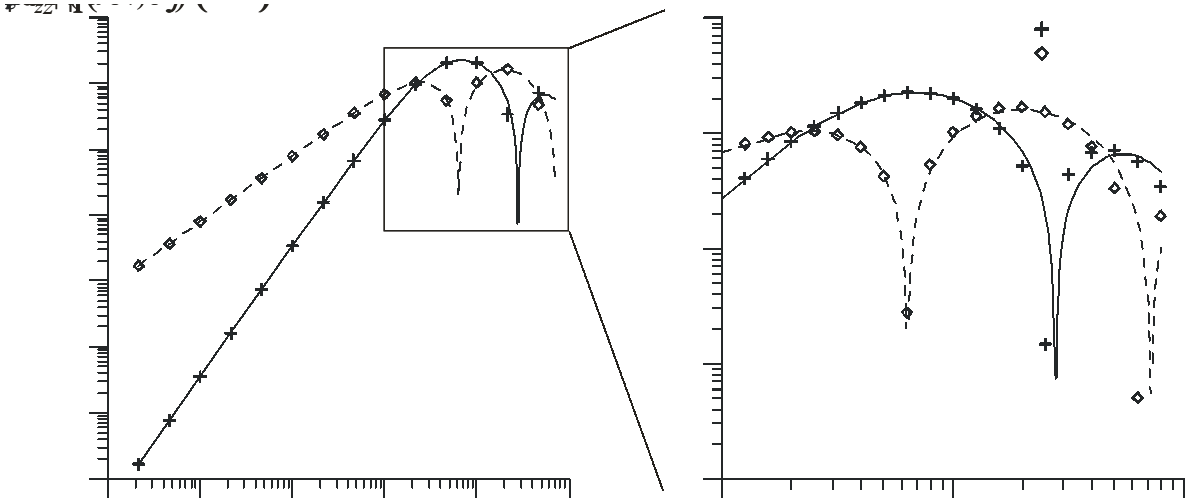

$$\sigma_2 / \sigma_1 = 10, \quad a = 6\ \text{m}, \quad b = 3\ \text{m}$$

Figure 5. The effect of conductivity contrast between body and background on the secondary magnetic fields. The operating frequency is 10^5 Hz, the source-receiver separation is 6 m and the horizontal hole-body separation is 3 m.

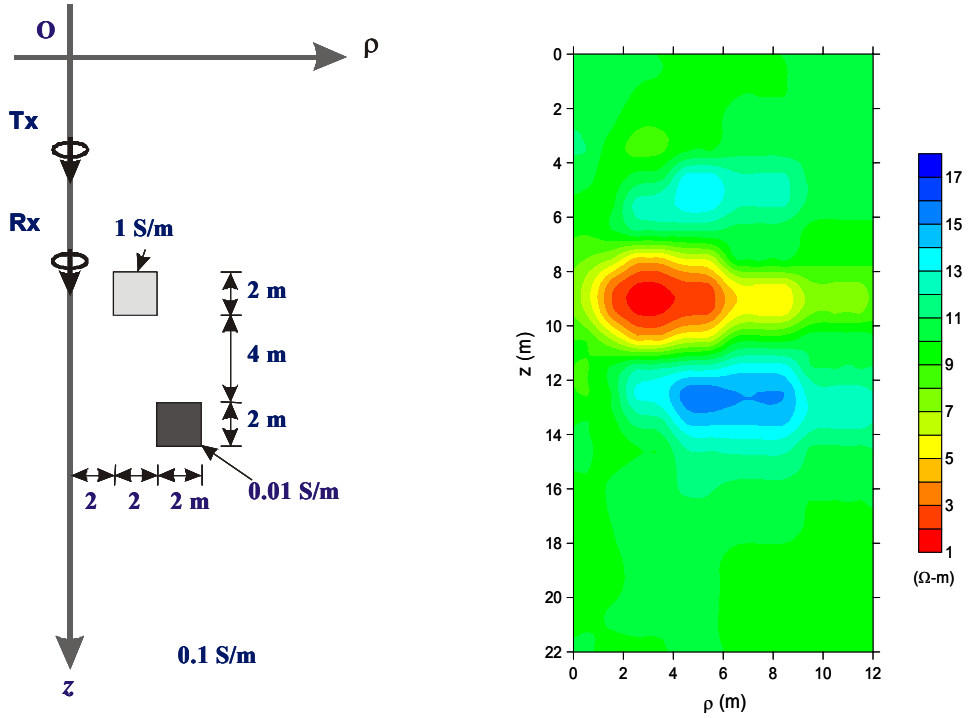

Figure 6. Inversion of synthetic model. The model (left) used to calculate synthetic data for inversion test consists of two bodies, of 1 S/m and 0.01 S/m, located in a whole-space of 0.1 S/m. An image of two conductors reconstructed from the synthetic data after 8th iteration.

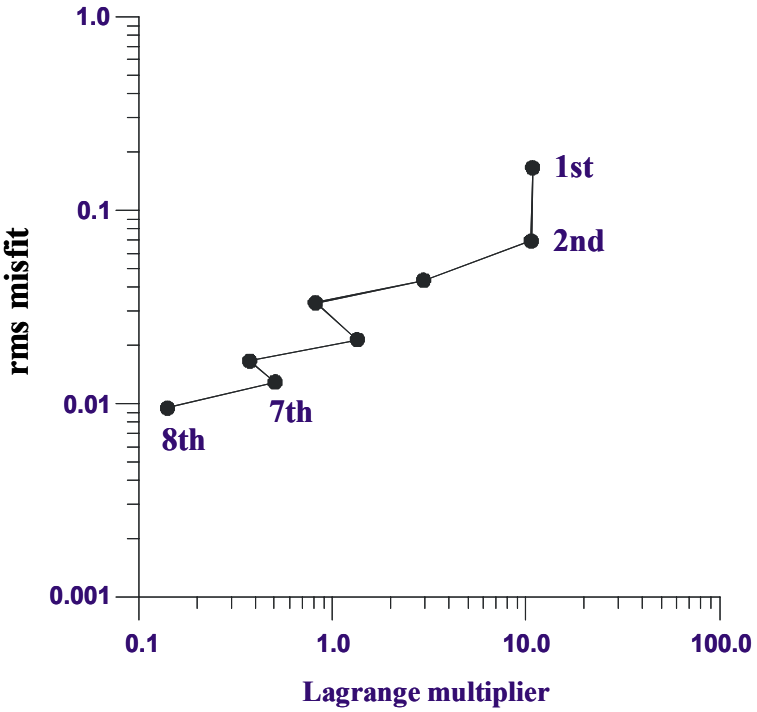

Figure 7. Convergence in rms for the synthetic model inversion.

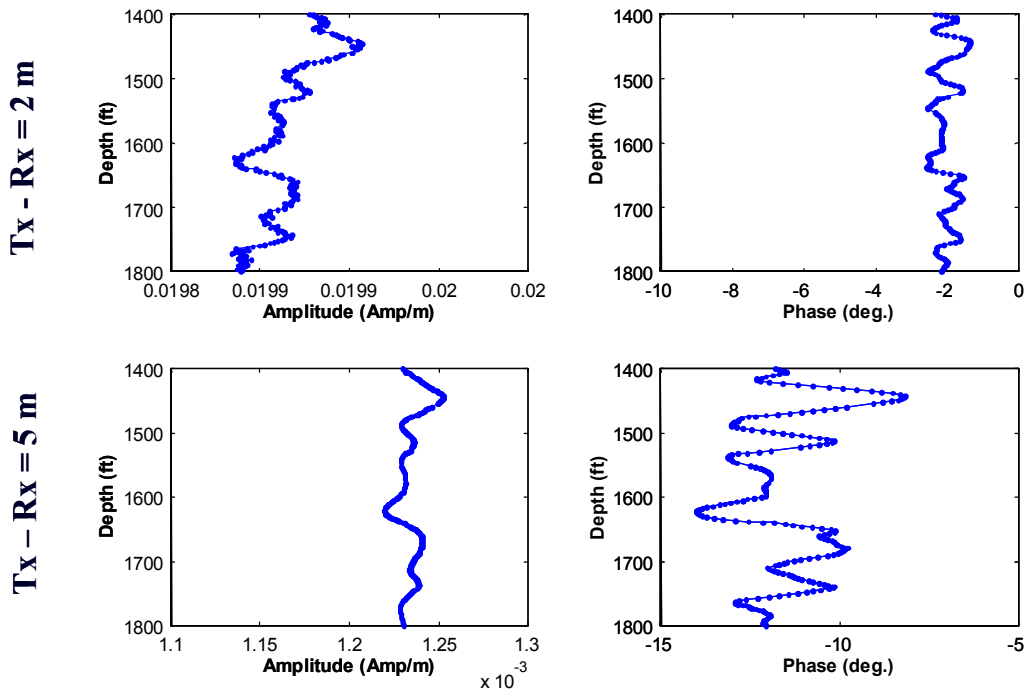

Figure 8. Vertical magnetic field data obtained in the borehole OBC1 at two offsets, 2 m and 5 m, at the frequency of 6 kHz. Source used is vertical magnetic dipole. These data sets are used to image electrical resistivity as shown in Figure 9.

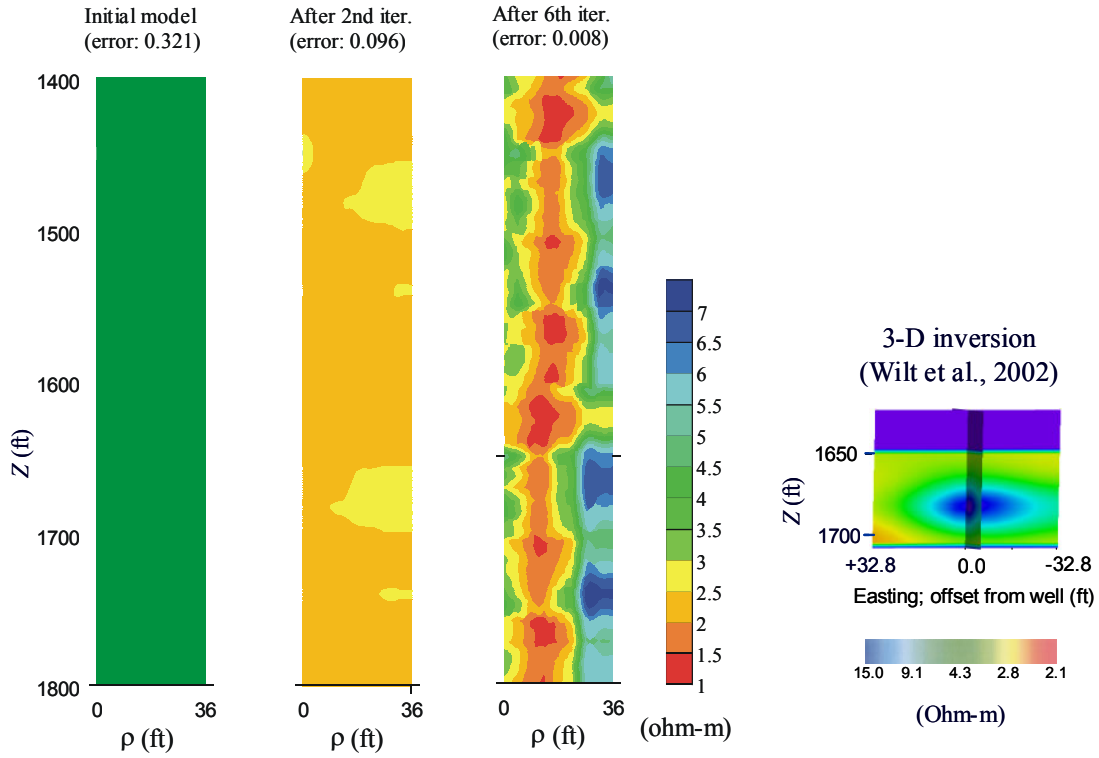

Figure 9. Resistivity imaging derived from the 2-D inversion of data obtained from Chevron USA. The model started with uniform conductivity of 0.25 S/m, and after eight iterations, the misfit in terms of rms (shown as fractional numbers after the number of iteration shown at the top of each image) converged to about 1%. The image shown on the right is from a 3-D inversion of three-component data with vertical magnetic dipole source (Wilt et al., 2002)

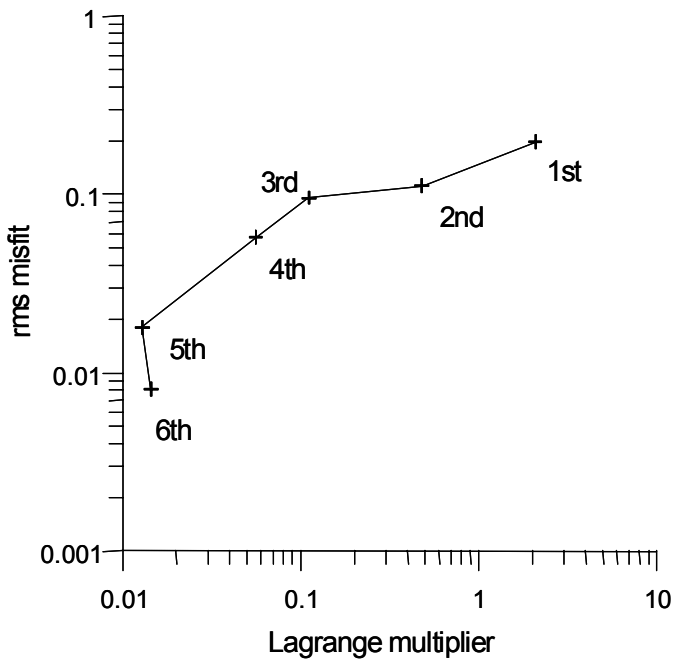

Figure 10. Convergence in rms misfit and associated Lagrange multiplier as a function of iteration during the inversion of field data

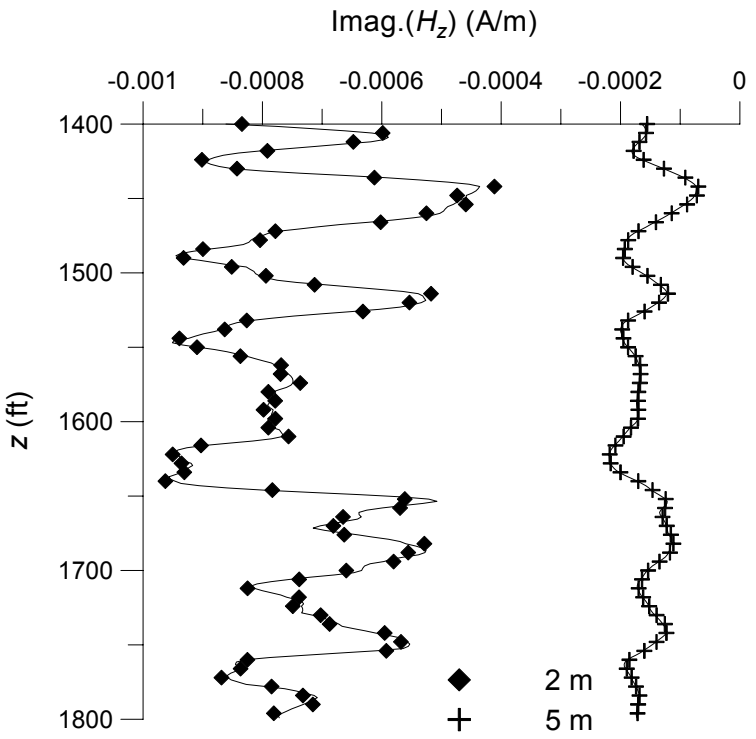

Figure 11. Comparison of field data and inverted model responses in the imaginary component.